Eur. Phys. J. A **21**, 243–255 (2004)
DOI 10.1140/epja/i2003-10204-2

THE EUROPEAN PHYSICAL JOURNAL A

The beta decay of neutron-deficient rhodium and ruthenium isotopes

S. Dean[a], M. Górska[b], F. Aksouh, H. de Witte, M. Facina, M. Huyse, O. Ivanov, K. Krouglov, Yu. Kudryavtsev, I. Mukha, D. Smirnov, J.-C. Thomas, K. Van de Vel[c], J. Van de Walle, P. Van Duppen, and J. Van Roosbroeck

Instituut voor Kern- en Stralingsfysica, University of Leuven, Celestijnenlaan 200 D, B-3001 Leuven, Belgium

Received: 26 November 2003 / Revised version: 12 January 2004 /

Communicated by J. Äystö

Abstract. The very neutron-deficient ^{91,92,93}Rh and ^{90,91}Ru nuclei were produced in ^{58}Ni(^{36,40}Ar, xn yp) fusion-evaporation reactions. Reaction products leaving the target were stopped in a gas cell and selectively laser ionised before mass separation using the LISOL setup. Data were collected in singles and coincidence formats to investigate β-delayed and isomeric γ decays. Ground-state decays of ^{91,93}Rh to excited states in the daughter nucleus were identified for the first time and the decay schemes of ^{90,91}Ru were expanded. The low-spin isomeric decay of ^{92}Rh was identified for the first time and detail added to the decay scheme of the known high-spin state. Results are discussed in terms of comparison with shell model calculations. β-delayed proton activity in the lighter ^{90}Rh and ^{89}Ru isotopes was also investigated and upper limits for this decay mode in these two nuclei have been included.

PACS. 23.40.-s β decay; double β decay; electron and muon capture – 21.10.-k Properties of nuclei; nuclear energy levels – 21.10.Tg Lifetimes – 21.60.Cs Shell model

1 Introduction

The study of neutron-deficient nuclei close to the $N = Z$ line has proven to be a rich source of nuclear-structure data. The nearby closed shells at $N = Z = 50$ make large-scale shell model calculations possible [1] allowing for a more complete comparison of not only level schemes but also of electromagnetic transition rates and Gamow-Teller strengths.

In this paper, results from β-decay studies on mass-separated samples of neutron-deficient Rh and Ru nuclei produced in heavy-ion fusion-evaporation reactions are reported. Because of the refractory nature of these elements, the reaction products were thermalised in a gas cell and laser ionised. The production of ion beams of these refractory elements has been enhanced by up to ~ 300 times relative to production without lasers. Elemental selective laser ionisation has thus enabled the β decay of ^{91}Rh and ^{93}Rh to be studied for the first time and has allowed a more detailed study of ^{92}Rh revealing, a previously only postulated, low-spin isomeric state. The decay scheme of ^{91}Ru has been expanded and detail added to that of ^{90}Ru. The half-lives determined in this study are compared to the theoretical predictions of Herndl and Brown [1] where they have been extracted from calculations of the Gamow-Teller strengths.

The following sections include a description of the experimental procedure along with particulars relating to the production of the refractory isotopes studied. Details of the analysis procedure are then presented followed by experimental results. The penultimate section contains a discussion of results as well as a comparison with theoretical calculations.

2 Experimental procedure

The neutron-deficient rhodium and ruthenium nuclei were produced in fusion-evaporation reactions at the Louvain-la-Neuve cyclotron facility in Belgium and mass separated using the LISOL facility [2]. Beams of $^{36(40)}$Ar$^{10+(11+)}$ typically of 1 eμA were released from the cyclotron at energies of between 235 and 255 MeV; the energy required having been calculated using the cross-section calculation code HIVAP [3] as the optimal for a particular reaction channel. A set of tantalum degraders of varying thicknesses was placed in the beam line to fine-tune the beam energy. A target of ^{58}Ni foil enriched to 99.93% and with a thickness of 4.4 mg/cm^2, was positioned inside a gas

---

[a] e-mail: `sarah.dean@fys.kuleuven.ac.be`

[b] *Present address*: Gesellschaft für Schwerionenforschung, Planckstrasse 1, D-64291 Darmstadt, Germany.

[c] *Present address*: VITO, IMS, Mol, Belgium.

Table 1. Laser wavelengths used for ionisation of rhodium and ruthenium atoms.

	$\lambda_{\text{first step}}$ (nm)	$\lambda_{\text{second step}}$ (nm)
Rh	232.258	572.55
Ru	228.538	553.09

cell [4,5]. Nuclei recoiling out of the target were stopped and neutralised within the cell by 500 mbar of purified Ar gas. Before being drawn out through the exit hole of the cell by a pressure differential, the reaction products were ionised selectively, according to Z, using two dye lasers tuned to the resonant atomic transitions of the particular element. On exiting the cell, laser-ionised nuclei and other surviving ions, were guided towards the LISOL mass separator by a sextupole ion guide [2] after which, surviving nuclei were implanted onto a movable tape at the centre of a detection setup.

The cyclotron and separator were pulsed in antiphase to counteract the detrimental effects of a high electron density present inside the gas cell when the beam is on [6]. In addition to this microcycle, a macrocycle, a beam-on followed by a beam-off period, was used to allow for accurate determination of half-lives. The on/off times were altered to suit the expected half-life of a particular isotope. A time-to-digital converter (TDC) was started at the beginning of each macrocycle recording the time of each triggered event relative to the start.

The laser system involved two excimer (XeCl) lasers (Lambda Physik LPX240i) of wavelength 308 nm that pump two dye lasers (Lambda Physik Scanmate 2). With a pulse width of 15 ns and a repetition rate of 200 Hz the lasers ionise atoms by way of a two-step process. Atomic electrons are first excited by laser photons to an excited, but still bound, intermediate level. A second laser frequency then excites to states lying above the ionisation limit. Excitation to autoionising states is used, as opposed to any route via the continuum, to exploit their more effective ionisation properties. The laser wavelengths used in this series of measurements are included in table 1, the particular atomic transitions associated with these energies however are not known.

The detection apparatus, described more fully in ref. [7], included two high-purity germanium detectors of 90% and 75% relative efficiency for γ-ray detection arranged in a compact configuration around β-sensitive plastic ΔE detectors of about 1.3 mm thickness that enclosed a tape station. Data were collected in singles and coincidence modes and are the accumulation of five separate experimental runs.

GEANT simulations [8] were used to calculate efficiency curves and to take into account true summing for high-multiplicity events; a consequence of the close geometry of the setup. Having built the decay scheme of a nucleus, every combination of prompt gamma-rays this scheme allowed was inserted, together with the relevant Q_{EC} value, into GEANT to determine absolute efficiencies for particular gamma-ray energies and to distinguish between sum peaks and crossover transitions. The justification for this contrived procedure can be seen in the difference between the efficiencies for the 511 keV gamma-ray shown in table 2.

Data were collected with the lasers on and, in order to facilitate the identification of resonantly produced γ lines, data were also collected without lasers. The acquisition times for the various measurements are included in table 2 along with the argon beam energies as incident on the target (E_{tar}). These were calculated using the ion transport code SRIM [9] and are included for completeness.

3 Isotope production

Production rates after mass separation of individual nuclei using resonant laser ionisation are shown in table 3 and are determined according to

$$\text{Yield} = \frac{A_{511} c_{\mathrm{d}} c_{\mathrm{c}}}{t_{\mathrm{cyc}} \eta_\beta \eta_\gamma I_{\mathrm{cyc}} t_{\mathrm{acq}}}.$$

The calculated yields are in units of at/eμC which is the number of nuclei implanted on the tape per electrical micro Coulomb of cyclotron beam. As β-branching ratios were unknown, the peak area of the 511 keV annihilation radiation line (A_{511}) was used to determine the yield. The intensity of the 511 keV line was corrected for decay contributions from both direct production of isobars and that via daughter decay. Account is taken of beam transport losses in the primary beam (t_{cyc}) and corrections to the beam dose are made so as to include only the time when the beam was actually on (c_{d}); *i.e.* half of the growing-in period. Not all nuclei implanted on the tape will necessarily decay within the measurement time but are included in the production rate nevertheless. This cycle correction (c_{c}) is defined as the ratio of the number of nuclei that are implanted on the tape to the number that decay in front of the detectors. The half-life of the nucleus must be determined before this correction can be calculated. Values for the cyclotron current (I_{cyc}) which is the dc current reading in a guarded Faraday cup just outside the gas cell and acquisition times (t_{acq}) and are listed in table 2. The final corrections (η_β and η_γ) are for detection efficiencies; for comparison, β-detection efficiency was typically 45% and for the 1.33 MeV ^{60}Co line the efficiency of the Ge detectors was 2.1%.

The efficiency of the ion source can be calculated if cross-sections for isotope production are known. The lack of predictive power however, of the present statistical fusion-evaporation codes (*viz* HIVAP [3] and PACE [10]) for absolute cross-sections for isotopes far from stability, precludes any meaningful conclusions. It should nevertheless be noted that the beam energies predicted to give the maximum values for production appear to be reliable. The experimental measurement of absolute isotope productions inside the gas cell provides an alternative to calculations. This has been done [11] and has placed the ion source efficiency at 2–3% and 0.2–0.6% for ^{95}Rh and ^{92,94,95}Ru, respectively. The nature of the technique

Table 2. A summary of the experimental parameters for each of the measured rhodium and ruthenium isotopes.

	Macrocycle on/off (s)	Lasers on t_{acq} (hr)	I_{cyc} (eμA)	Lasers off t_{acq} (h)	I_{cyc} (eμA)	η_{511} within decay scheme (%)	E_{tar} (MeV)
^{93}Rh	30/50	20.37	1.0	2.66	0.9	6.0(3)	171
^{92}Rh	12/20	8.26	2.2	11.0	1.6	3.2(2)	135
^{91}Rh	12/20	20.9	2.0	2.87	1.6	4.6(2)	158
^{91}Ru	12/20	3.08	2.1	2.87	1.6	5.6(3)	158
^{90}Ru	32/32	2.13	1.0	1.07	1.0	6.4(3)	180

Table 3. Performance of the ion source and selectivity values for each of the measured nuclei.

Nucleus	Yield from mass separator (at/eμC)	Selectivity	Reaction exit channel
^{93}Rh	31(7)	> 70	^{58}Ni(^{40}Ar^{11+}, p4n)
^{92}Rh	21(4)	> 310	^{58}Ni(^{36}Ar^{10+}, p1n)
^{91}Rh	24(4)	> 26	^{58}Ni(^{36}Ar^{10+}, p2n)
^{91}Ru	441(59)	15(3)	^{58}Ni(^{36}Ar^{10+}, 2pn)
^{90}Ru	16(4)	2.6(8)	^{58}Ni(^{36}Ar^{10+}, 2p2n)

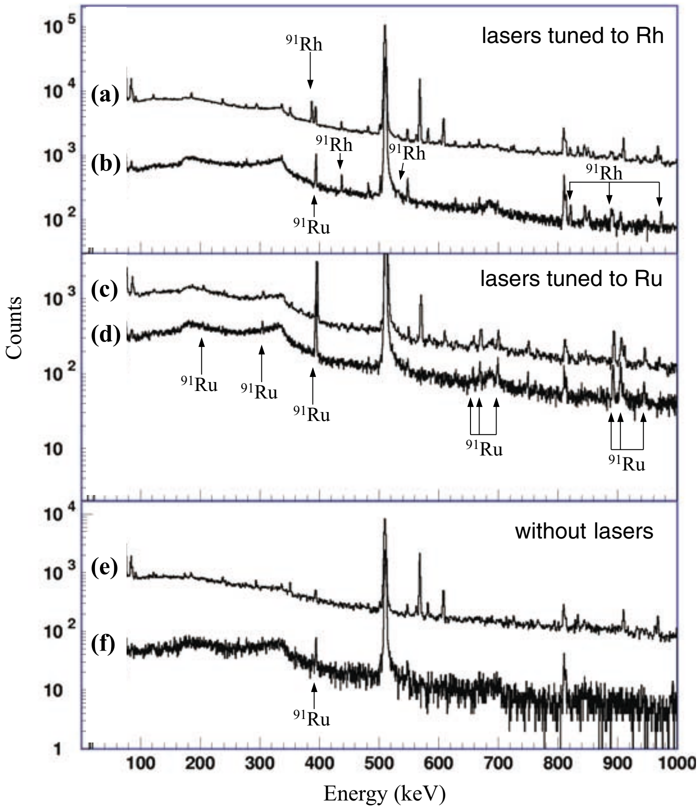

Fig. 1. A section of the mass 91 gamma-ray spectra with (a) data collected with lasers tuned to rhodium in singles mode and (b) β-gated. (c) With lasers tuned to ruthenium in singles mode and (d) β-gated. Without lasers: singles (e) and β-gated (f). The spectra in different panels were taken for different times (see table 2).

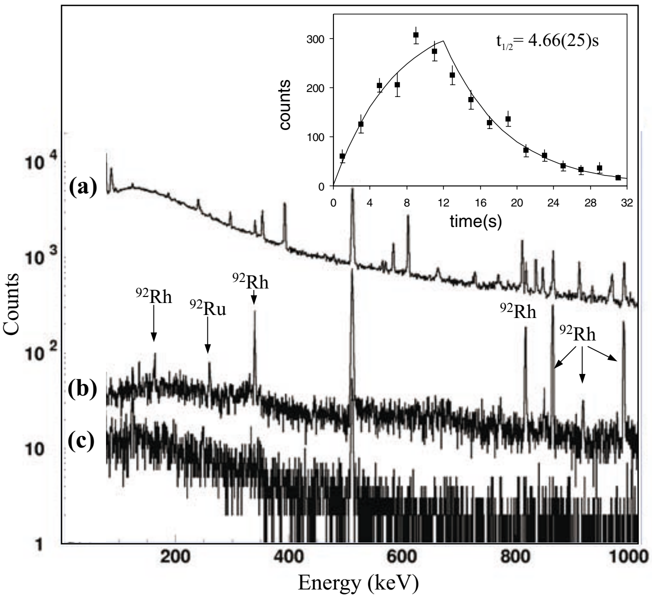

Fig. 2. A section of the mass 92 γ-ray spectra with (a) data collected in singles mode and lasers tuned to rhodium, (b) with lasers again but β-gated and (c) without lasers and β-gated. Inset: A half-life fit to the time behaviour of the 163, 340, 818, and 991 keV γ lines.

means that efficiencies for the shorter-living isotopes such as those studied here could not be determined however, since the half-lives of the isotopes in this study are still long compared to the evacuation time of the gas cell [4, 5] the same efficiency is expected. The discrepancy between the ion source efficiencies for rhodium and ruthenium may be attributable to the quality of the ionisation procedure for each element. Only for rhodium was a filament available inside the gas cell beforehand to produce stable rhodium atoms allowing fine tuning the ionisation procedure. Certainly this explanation is borne out by values for selectivity which is the ratio of isotope production with and without lasers.

Figures 1 and 2 serve to highlight the advantages of this laser ionisation technique in combination with β gating. Without lasers, the singles spectrum (fig. 1(e)) is dominated by γ lines coming from room and neutron-induced backgrounds. Requiring a coincident β-particle drastically reduces this background (cf. fig. 1(f)). The use of lasers, tuned to rhodium and ruthenium, strongly enhances the ionisation and thus extraction of these nuclei resulting finally in increased count rates in the γ lines of these nuclei as they decay. A comparison between singles and β-gated spectra can also be used to detect events which are not promptly correlated with β-particles, such as isomeric decay. An example of such a γ line, seen at 387 keV in fig. 1(a), is firmly associated with the production of ^{91}Rh by virtue of its absence from fig. 1(e), the singles spectrum without lasers.

4 Analysis and data reduction

A comparison of data taken with and without lasers was used in the first instance to identify γ lines which may be attributable to the decay of resonantly produced nuclei or their subsequent daughter decay; the rationale being that only those lines present or enhanced using lasers are the result of elemental selective photoionisation in the gas cell. Individual γ lines were then assigned to either mother or daughter decay by virtue of their half-life behaviour. Time gates on TDC spectra allowed the time evolution of peak areas to be followed as they passed through the growing-in and decay stages of each macrocycle. This time behaviour was then fitted using the function minimisation and error analysis program *MINUIT* [12].

The β-feeding (I_β) to ground and excited states in the daughter nucleus was calculated using the 511 keV annihilation line. Counts in this line due to β-decaying isobars were subtracted and the remainder attributed to the nucleus in question. A fit to the time behaviour of the 511 keV line was used as a check of this procedure. A note of caution regarding the β-branching ratios; the large amount of energy available for β decay for nuclei in this region suggests a significant possibility of feeding to highly excited states which subsequently decay to the observed lower-lying levels. This would compromise the integrity of the calculated branching ratios and mean that the log*ft* values given should be regarded as lower limits. Values for β-branching to the groundstate of the daughter are particularly vulnerable to this problem. Since all 511 keV counts that cannot be associated with γ events visible in the γ-ray spectra are assigned to ground-state decay, weakly populated states and branching to states producing γ-rays outside the 4 MeV γ-energy range may be wrongly attributed to ground-state decay. A further consequence may be that apparently forbidden β decays, *e.g.* the $(13/2^+)$ state populated in ^{91,93}Rh decay, may result from γ transitions from higher-lying levels fed by allowed β transitions. The construction of level schemes was based on γ-γ coincidence matrices and log*ft* values were calculated using $Q_{\rm EC}$ values from mass excesses taken from ref. [13].

5 Results

5.1 ^{93}Rh

An argon beam initially at 250 MeV was used in the ^{58}Ni(^{40}Ar, p4n) reaction to produce ^{93}Rh nuclei allowing for the first time, the β decay of this nucleus to be studied. A beam energy of 171 MeV in front of the target coincided with the maximum calculated cross-section from HIVAP of 169 μb for this particular reaction channel. Prior to this study, the level structure of ^{93}Ru had been studied by in-beam spectroscopy experiments for example for the first time by [14] using a ^{92}Mo(α, 3n)^{93}Ru reaction. A line corresponding to that observed here at 1393.3 keV was identified then as belonging to a $(13/2^+)$–to–ground-state transition. This result was compatible with a later measurement [15] using the ^{58}Ni(^{40}Ca, 4pn)^{93}Ru reaction.

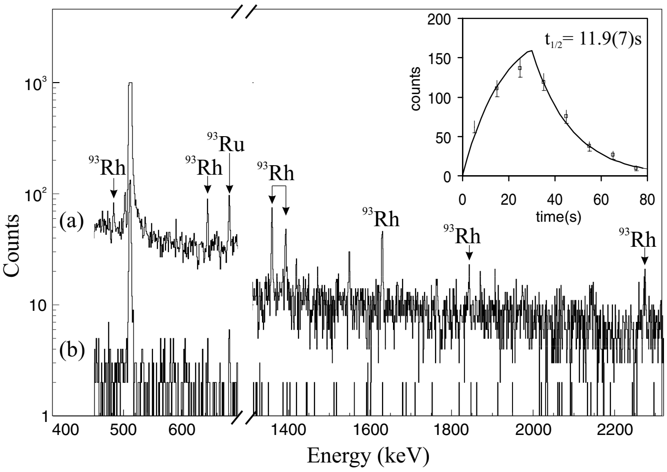

Fig. 3. γ-ray spectra for $A = 93$ (a) β-gated with lasers tuned to rhodium and (b) β-gated without lasers. Inset: growing in and decay fit to the time behaviour of the sum of the seven lines attributed to ^{93}Rh decay.

Figure 3 shows the β-gated spectra at mass 93 accumulated during three separate measurements. In addition to the 1393 kev line observed in in-beam studies, six additional γ lines could be unambiguously assigned to ^{93}Rh decay. No evidence is seen of the ^{93}Ru$(1/2^-)$ 10.8 s isomeric decay as described in ref. [16]; neither the $M4$ isomeric transition nor any β-delayed γ events. The $(1/2^-)$ state was thus either weakly or not populated in the (^{40}Ar, p4n) reaction. Figure 4 shows the decay scheme resulting from the analysis of γ-γ coincidence spectra. The peak areas, energies and intensities of the seven γ lines are included in table 4.

β-branching (I_β) was determined using the 511 keV annihilation line. Counts due to the decay of ^{93}Ru with its half-life of 59.7(6) s were calculated using the 680.7(9) keV line with $I_\beta = 5.9(4)\%$ [16]. The calculated amount was then subtracted from the total 511 keV area and the remainder attributed to ^{93}Rh. The ^{93}Rh production, as determined using the 511 keV line, was 31(7) at/eμC.

The half-life was calculated from a fit to the sum of the individual TDC spectra gated on each of the seven lines attributed to ^{93}Rh and is shown in the inset to fig. 3.

5.2 ^{92}Rh

The level structure of ^{92}Ru has been previously investigated by both in-beam [17–20] and β-decay spectroscopy [21]. The results presented here are in agreement

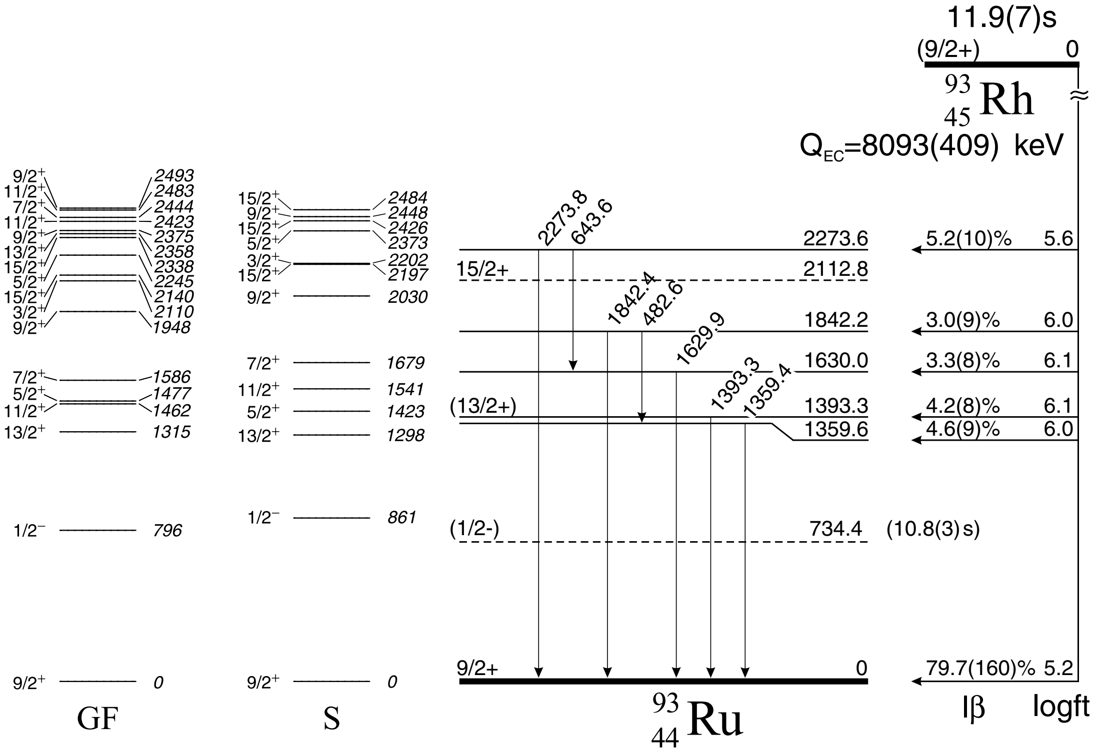

Fig. 4. The decay scheme of ^{93}Rh with shell model predictions. The calculated states include only those with $I^{\pi} \leq 15/2^{+}$ below 2.5 MeV. The $(1/2^{-})$ and $15/2^{+}$ states detailed in refs. [16] and [15], although not seen in this study, are included for purposes of comparison.

Table 4. Energies, peak areas and relative intensities of β-gated γ-rays assigned to ^{93}Rh decay.

E_{γ}(keV)	A_{γ}	Relative intensity
482.6(3)	70(23)	20(7)
643.6(1)	118(16)	42(8)
1359.4(1)	179(18)	100
1393.3(2)	130(16)	72(14)
1629.9(1)	147(15)	98(19)
1842.4(6)	45(18)	31(13)
2273.8(9)	60(13)	48(13)

with the most recent in-beam study [20] except for the placement of the 919 keV line and the inclusion here of a 340 keV line (also reported in the earlier [18]). The level scheme reported by [21] has been expanded and developed here by the addition of three γ lines and their respective levels as well as feeding to these levels.

The ^{58}Ni(^{36}Ar, pn) reaction was used to produce ^{92}Rh nuclei which had a HIVAP calculated maximum cross-section of 368 μb at 120 MeV which occurred close to the centre of the target. Figure 2 shows γ-ray spectra acquired at mass 92.

A calculation of feeding to the observed levels based on the 511 keV annihilation line puts feeding to the ground state of ^{92}Ru ($I^{\pi} = 0^{+}$) and the 2^{+} 866 keV level at no less than 25% and 5%, respectively. This is inconsistent with the assigned ground-state spin and parity of ($\geq 6^{+}$) for ^{92}Rh [21]. This apparent discrepancy may be explained by the decay of a low-spin isomeric state in ^{92}Rh. As fig. 5 shows, there is evidence for two half-life components in the time behaviour of the 866 keV line.

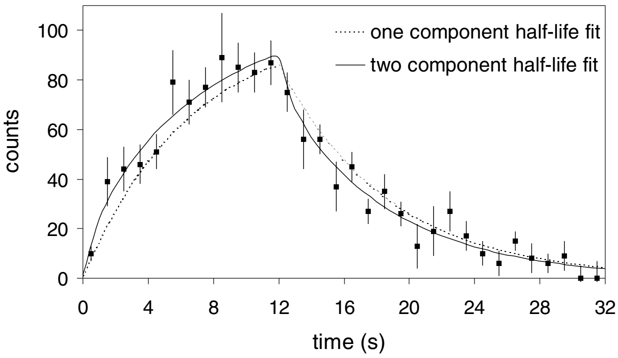

Fig. 5. A one-component half-life (dashed line) and two-component half-life (solid line) fit to the time behaviour of the 866 keV line. See text for details.

The half-life of the longer-living ($\geq 6^{+}$) state in the two-component fit has been fixed at 4.66(25) s which was determined from the time behaviour of the 163, 340, 818 and 919 keV lines. This gives the low-spin isomer a half-life of 0.53(37) s. In view of this and an examination of γ-γ coincidence matrices, the level scheme shown in fig. 6 is proposed. The half-life of the 8^{+} state was measured

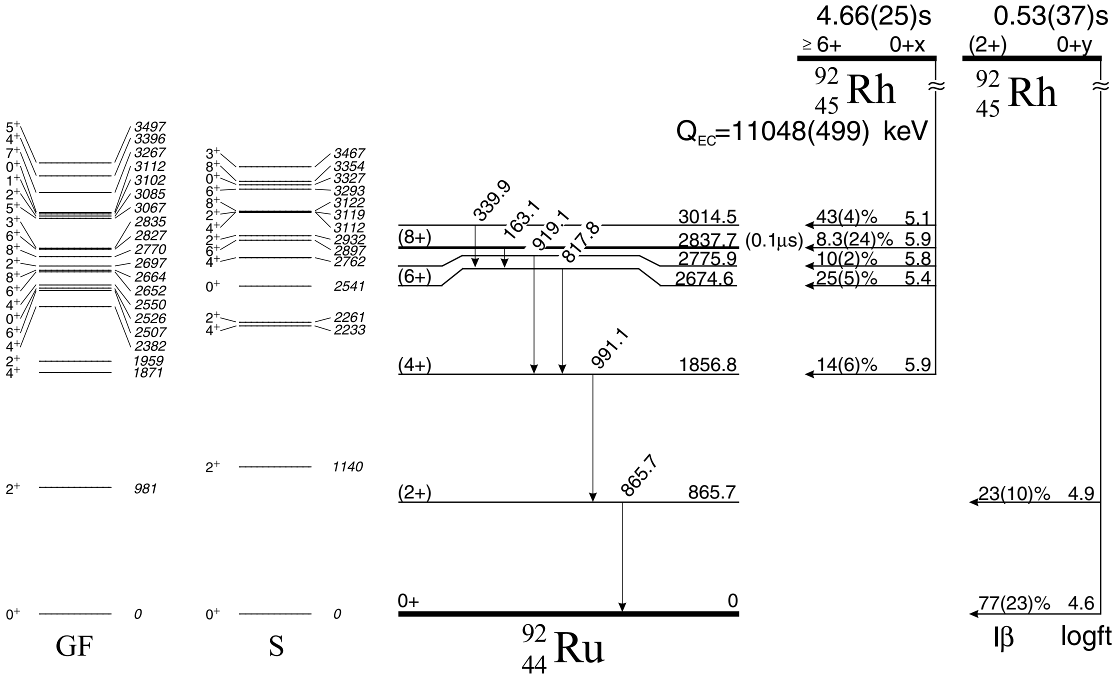

Fig. 6. The decay scheme of ^{92}Rh with shell model predictions. All calculated levels below 3.5 MeV with $I^\pi \leq 10^+$ are included.

Table 5. Energies, peak areas and relative intensities of β-gated γ-rays assigned to ^{92}Rh decay.

E_γ(keV)	A_γ	Relative intensity ^{92}Rh($\geq 6^+$)
163.1(2)	238(52)	6.8(20)
339.9(2)	921(19)	43(4)
817.8(1)	889(41)	76(9)
865.7(1)	1207(85)	103(15)
919.1(1)	120(25)	10(2)
991.1(3)	1055(29)	100
		^{92}Rh(2^+)
865.7(1)	219(78)	100

Table 6. Energies, peak areas, relative intensities and half-lives of γ-rays assigned to ^{91}Rh decay. The proximity of the 511 keV line meant that it was not possible to determine the half-life of the 533 keV line; suffice to say it was short and similar to the others.

E_γ (keV)	A_γ	Relative intensity	Half-life (s)
437.7(1)	854(67)	100	1.65(30)
533.3(1)	156(78)	21(10)	
821.1(1)	334(32)	63(9)	1.84(35)
889.8(2)	268(49)	52(11)	1.40(33)
973.1(1)	297(43)	61(11)	1.52(29)
387.4(2)	8066(242)$^{(a)}$	351(39)	1.46(11)

(^{a}) Peak area taken from singles spectra.

to be 100(14) ns [17] and is included in the level scheme. It should be noted that although the ($\geq 6^+$) state has been thus far referred to as the ground state, it is not yet apparent that this is indeed the case hence the energy values ($0 + x$ and $0 + y$) of the two states in fig. 6.

The properties of the individual lines attributed to the decay of ^{92}Rh are listed in table 5. The 866 keV line had a total area of 1426(34) and counts were apportioned between the low- and high-spin decays on the basis of the two-component half-life fit shown in fig. 5.

5.3 ^{91}Rh

^{91}Rh nuclei were produced in the ^{58}Ni(^{36}Ar, p2n) reaction allowing the β decay of this nucleus to be studied for the first time. The argon beam, initially at 235 MeV, was degraded to 121 MeV close to the centre of the target, overlapping with the maximum cross-section of 11 μb for this reaction channel as calculated by HIVAP. The five γ lines indicated in the β-gated γ-ray spectra shown in fig. 1(b), have been assigned to the decay of ^{91}Rh (see table 6). An examination of γ-γ matrices gated on these transitions was unable to reveal any coincidences between the lines.

Apart from a recent half-life measurement [22], ^{91}Rh was unknown experimentally prior to this study. A ground state of $9/2^+$ is however favoured based on systematics and shall be adopted as a tentative assignment here. The better known ^{91}Ru has been tentatively assigned to have a ground state with $I^\pi = 9/2^+$ [23] which would agree with the systematic properties of $N = 47$, $Z =$ even nuclei in the vicinity. Both assignments are consistent with the β-decay branchings reported here.

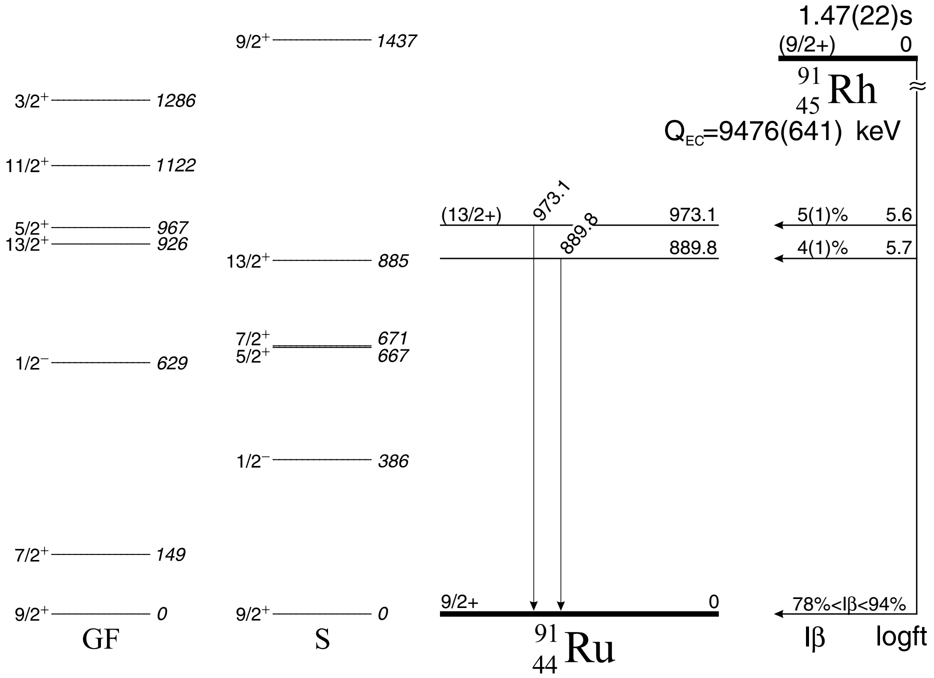

Fig. 7. The decay scheme of ^{91}Rh including only two of the six γ lines associated with ^{91}Rh decay. The reasons for this and the limits on feeding to the ground state in ^{91}Ru are given in the text. The shell model calculations include only those levels with $I^{\pi} \leq 15/2^{+}$ below 1.5 MeV.

Earlier in-beam experiments exploring the excited states of ^{91}Ru [24,25] have attributed a 973 keV line to a $(13/2^{+})$–to–ground-state transition and a very recent measurement [26] indicates a line at 890 keV to result from an $(11/2^{+})$–to–ground-state transition. For this reason, and others that will be discussed in sect. 6.4, only these two γ lines, out of the six listed in table 6, are placed in the level scheme shown in fig. 7. Excepting the γ line at 533 keV, half-lives based on the time behaviour of each of the lines were determined and are also included in table 6 along with their peak areas and intensities which have been normalised to the 438 keV line. The half-life attributed to ^{91}Rh ground-state decay was established as 1.47(22) s from a weighted mean of the values for the 890 and 973 keV lines. This is in agreement with the previous measurement of 1.7(2) s [22].

The singles spectra in fig. 1 reveal another feature of ^{91}Rh decay. The line at 387 keV is not seen in β-gated spectra with or without lasers. It is however strongly produced in the singles spectra but only when the lasers are tuned to rhodium. This establishes an isomeric transition in either ^{91}Rh or ^{91}Ru; the former being fed directly in the heavy-ion reaction and the latter populated through the decay of ^{91}Rh. The γ-ray intensity of this line represents a production rate of 4.0(8) at/eμC.

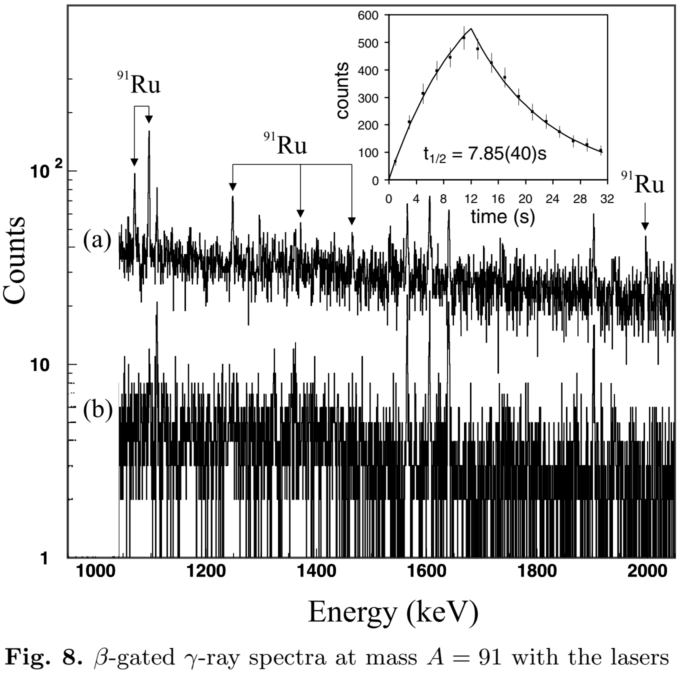

Fig. 8. β-gated γ-ray spectra at mass $A = 91$ with the lasers tuned to ruthenium (a) and without lasers (b). Inset: A half-life fit to the time behaviour 394 keV line from the decay of ^{91}Ru.

5.4 ^{91}Ru

Figures 1 and 8 show mass-91 spectra resulting from of 3.08 hours irradiation of ^{58}Ni by a 158 MeV ^{36}Ar beam. From HIVAP calculations, a maximum cross-section of 28 mb is obtained from a beam energy of 130 MeV. The incident ^{36}Ar beam reaches this value close to the middle of the target. As detailed in the previous section, the ground state of ^{91}Ru has been assigned $9/2^{+}$ with an

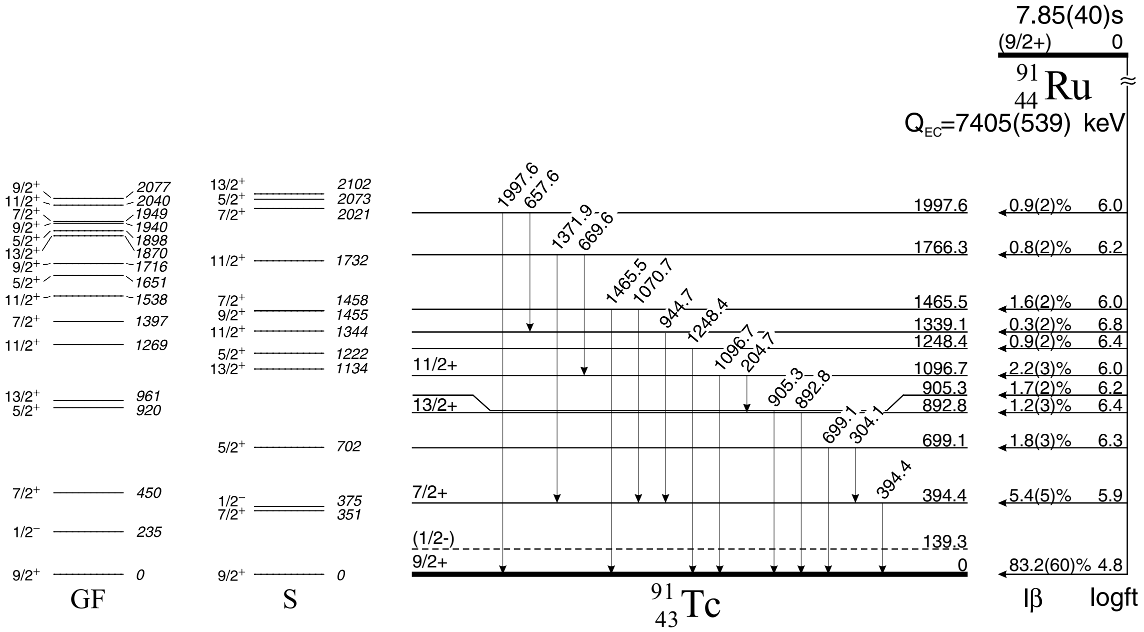

Fig. 9. The decay scheme of ^{91}Ru with shell model predictions. The calculated states include those with $I^{\pi} \leq 15/2^{+}$ below 2.2 MeV. The $(1/2^{-})$ state, observed in [28] is included for comparison.

Table 7. Energies, peak areas and relative intensities of β-gated γ-rays assigned to ^{91}Ru decay.

E_{γ}(keV)	A_{γ}	Relative intensity
204.7(3)	246(97)	3.9(23)
304.1(1)	364(70)	11(2)
394.4(1)	4534(118)	100
657.6(2)	113(34)	7.2(23)
669.6(2)	152(55)	8.5(26)
699.1(1)	331(50)	21(5)
892.8(4)	420(91)	21(6)
905.3(3)	535(47)	32(4)
944.7(1)	166(30)	5.6(30)
1070.7(1)	246(25)	19(3)
1096.7(1)	627(34)	37(5)
1248.4(1)	226(32)	17(3)
1371.9(2)	65(23)	6.1(22)
1465.5(3)	110(36)	9.5(33)
1997.6(9)	139(29)	9.5(22)

isomeric $(1/2^{-})$ state identified as a β-delayed proton precursor [27]. The excitation energy of this state is unknown and the $(1/2^{-})$ assignment was based on systematics in $N = 47$ nuclei and statistical model calculations of proton energy spectra. There is no evidence however in the present study of the subsequent ^{90}Mo decay in the γ-ray spectrum that would indicate β-delayed proton emission in this nucleus.

Three previous in-beam studies [23,24,28] identified the four lowest-lying $7/2^{+}$, $9/2^{+}$, $11/2^{+}$ and $13/2^{+}$ levels in ^{91}Tc and, in addition to these four known lines, eleven new γ lines were attributed to the decay of ^{91}Ru and added to the existing scheme as shown in fig. 9. The properties of these lines are included in table 7.

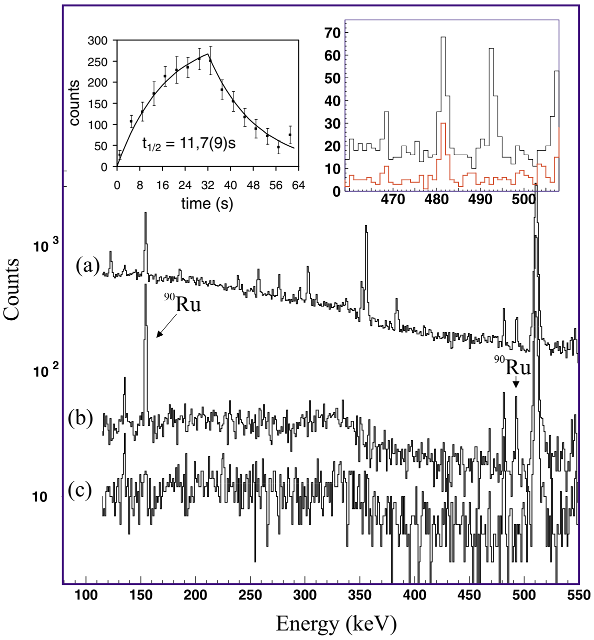

Fig. 10. γ-ray spectra for $A = 90$ with (a) lasers tuned to ruthenium in singles (b) β-gated and (c) β-gated without lasers. Left inset: a half-life fit to the time behaviour of the 154 keV line. Right inset: magnification of the region around 490 keV with and without lasers.

A half-life of 7.85(40) s was assigned to the decay of this nucleus based on a fit to the time behaviour of the most intense 394 keV line, shown in the inset to fig. 8, and is in agreement with a previous measurement of 9(1) s [23].

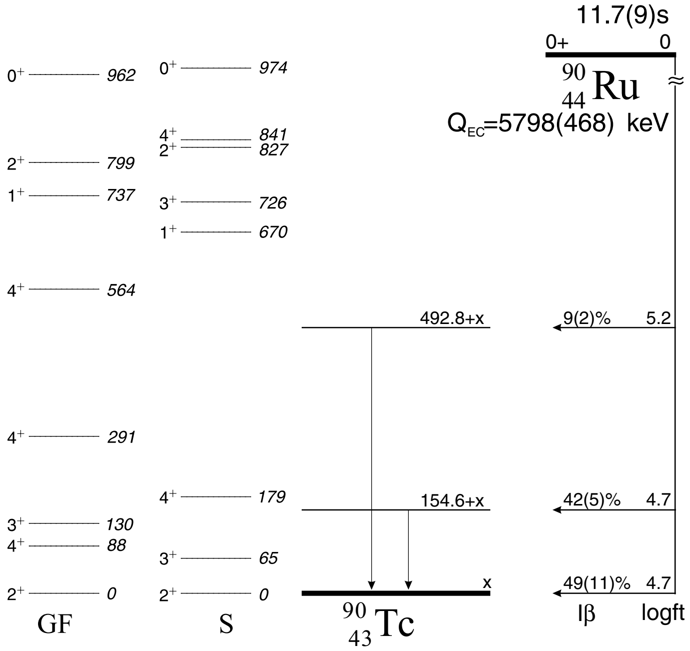

Fig. 11. The decay scheme of ^{90}Ru with shell model predictions. The calculated levels include those with $I^{\pi} \leq 4^{+}$ below 1 MeV. The lowest-lying observed level is aligned to the 2^{+} states seen in fig. 14 below and since this is almost certainly not the ground state, the observed level energies are quoted as relative to "x".

5.5 ^{90}Ru

A ^{36}Ar beam at 180 MeV incident on target proved to be the energy best suited to production of ^{90}Ru agreeing with HIVAP calculations for a maximum cross-section of 2.4 mb at an energy 150 MeV in the middle of the target. Figure 10 shows the results of data collected at mass 90.

The line at 154.6 keV was identified in an earlier measurement along with 37 others as belonging to the decay of ^{90}Ru [29]. The line reported there at 491.8 keV is probably that placed here at 492.8 keV. No evidence is seen of the remaining 36 lines. The γ-γ matrices show the two lines to be uncorrelated, they are thus placed as the parallel transition shown in fig. 11.

This nucleus was measured on two occasions, the first occasion using a higher beam energy produced a larger amount of isobaric contamination effectively obscuring the 492.8 keV line which is clearly visible in fig. 10 (right inset). The 154.6 keV line however, being more intense, was seen with an area of 1595(94) counts. This data was summed with data from the later experiment and was used to determine the half-life of ^{90}Ru as shown in fig. 10 (left inset). Branching to excited states was calculated from the data of the later experiment only and the properties of the γ lines for that run are included in table 8.

Table 8. Energies, peak areas and relative intensities of β-gated γ-rays assigned to ^{90}Ru decay.

E_{γ}(keV)	A_{γ}	Relative intensity
154.6(1)	810(46)	100
492.8(1)	81(12)	21(4)

5.6 β-delayed proton activity

As a natural extension to this work, a study of β-delayed proton activity in the lighter nuclei in this region was investigated. Calculations of the energetics of such decays as well as supporting literature encouraged this enterprise. For this set of measurements, the mass-separated beam was implanted into a thin carbon foil in front of a ΔE-E Si telescope system with thicknesses of 30 and 700 μm, respectively. Protons can thus be readily identified in a plot of energy loss in the ΔE section *versus* the remaining energy deposited in the E detector. The high efficiency of this detection system as compared with γ-ray detection together with the increasing probability of such decays as the drip line is approached make this a powerful tool for extracting nuclear-structure information where present production rates preclude γ-ray spectroscopy. The telescope was housed inside a vacuum chamber attached to the beam line with a 75% relative efficiency HPGe detector placed directly behind it.

Five hours of data taken on ^{89}Ru failed to produce any protons. This result differs from that of an earlier measurement using the same reaction [30]. In that study, a 741 keV line from the $2^{+} \rightarrow 0^{+}$ transition in ^{88}Mo was seen in coincidence with events in a Si detector however, in the absence of mass separation and a particle identification setup, as was the case in ref. [30], there is always the possibility that the 741 keV line is a result of ^{89}Tc decay.

No evidence of ^{89}Ru decay was seen either in γ-ray or proton spectra however, an upper limit on I_{p}, the β-delayed proton branching, can still be calculated. The production of ^{89}Ru is derived by scaling the production of ^{90}Ru down by a factor $\sigma(^{90}\mathrm{Ru})/\sigma(^{89}\mathrm{Ru})$, where $\sigma(^{90}\mathrm{Ru})$ and $\sigma(^{89}\mathrm{Ru})$ are cross-sections for ^{90}Ru and ^{89}Ru calculated using HIVAP. This results in $I_{\mathrm{p}} < 0.15\%$ for ^{89}Ru in the one-σ limit.

β-delayed proton emission from the $N = Z$ nucleus ^{90}Rh was also measured resulting in three protons over a period of 2.7 hours. A similar calculation to that above gives $I_{\mathrm{p}} < 0.4\%$. It was not possible to determine a half-life based on these three events however, based on their time distribution, ^{90}Rh ground-state decay measured in ref. [22] can be ruled out on account of its short half-life; 12^{+9}_{-4} ms. The timing of the observed particles is nevertheless consistent with the decay of a longer-living isomeric state in ^{90}Rh also reported in ref. [22] with a half-life of $1.0^{+0.3}_{-0.2}$ s.

6 Discussion

6.1 Introduction

Experimental level schemes have been compared with theoretical model calculations and are shown in figs. 4, 6, 7, 9 and 11 to 14. These calculations were performed with the shell model code ANTOINE [31]. For the calculations indicated "GF", the empirical two-body matrix elements of the residual interaction and the four single-particle energies were taken from Gross and Frenkel [32]. Here proton and neutron holes are restricted to the ($p_{1/2}$, $g_{9/2}$) single-particle orbits. The parameters for this interaction were calculated from a fit to the energy levels in ten nuclei with $N = 48,49,50$. The levels labelled "S" , refer to calculations performed using the interaction parameters of Sinatkas *et al.* [33,34] who assume a ^{100}Sn inert core and consider proton and neutron holes distributed in the $g_{9/2}$, $p_{1/2}$, $p_{3/2}$ and $f_{5/2}$ orbitals of that many-body system.

Proton-rich nuclei in the range $A = 86$–100 have also been investigated by Herndl and Brown [1] within the ($p_{1/2}$, $g_{9/2}$) space using the SLGT0 interaction taken from ref. [35] which is essentially identical to that of Gross and Frenkel. Half-lives were determined from the calculated Gamow-Teller matrix elements reduced by an orbit-dependent quenching factor $q = 0.4$ where, $(\sigma\tau)_{\mathrm{reduced}} = (1-q)(\sigma\tau)$. The resulting values along with those determined experimentally are included in table 9. With the exception of ^{90}Ru and ^{92}Rh, the predicted half-lives are in remarkably good agreement with those measured although, a general tendency to overestimate the experimental values should be noted. The predicted half-life for ^{92}Rh(2^+) state shows a much better agreement with the measured half-life for ^{92}Rh($\geq 6^+$) than it does with the shorter-living (2^+) state.

Table 9. Experimental half-lives determined in this study along with previous measurements and theoretical predictions where available. All values are in seconds.

Nucleus	Present study	Previous work	Theory [1]
^{93}Rh	11.9(7)	13.9(16) [22]	14.9
^{92}Rh(2^+)	0.53(37)		4.30
^{92}Rh($\geq 6^+$)	4.66(25)	5.6(5) [22]	
^{91}Rh($9/2^+$)	1.47(22)	1.7(2) [22]	1.68
^{91}Rh($1/2^-$)	1.46(11)		
^{91}Ru	7.85(40)	9(1) [23]	12.3
^{90}Ru	11.7(9)	11(3) [29]	41.5

6.2 ^{93}Rh decay

Many of the low-lying states in ^{93}Ru populated in the β decay of ^{93}Rh can be understood as belonging to $\pi(p_{1/2},g_{9/2})^{-6}\nu g_{9/2}^{-1}$ configurations. Figure 4 shows the results of shell model calculations up to 2.5 MeV alongside the experimental levels observed in β decay. The calculated multiplet of states resulting from the single neutron hole coupled to proton 2^+ excitations in the corresponding $N = 50$ nucleus correspond well with the five states observed between 1 and 2 MeV. The state at 2273 keV with its lower log*ft* value is a likely candidate for the first-excited $9/2^+$ state calculated in both model spaces to lie around 2 MeV.

The idea that the $p_{1/2}$ and $g_{9/2}$ orbitals are the major players in the construction of the observed excited states is supported by the remarkable similarity between the two shell model calculations. Neither valence space predicts any excited positive-parity state at a lower energy than the $13/2^+$. The $1/2^-$ state, unobserved in this study, is included in the decay scheme and shell model calculation for comparison.

6.3 ^{92}Rh decay

The shell model calculations for excited states in ^{92}Ru are in good agreement with experimentally observed levels as fig. 6 shows. The agreement is particularly good for the GF calculation where the difference between observed and calculated excitation energy does not exceed 200 keV. The calculation using the Sinatkas interaction although still satisfactory, tends to overestimate the excitation energy of all the experimental levels by about 250 keV.

The experimental evidence for a second β-decaying state in ^{92}Rh presented earlier is corroborated by the shell model calculations shown in fig. 12. The experimental data is that from Kast *et al.* [36] and is presented with the shell model calculations both of which predict a 2^+ ground state about 50 keV below a 6^+ state. This state would be a good candidate for the observed decay of a low-spin state.

6.4 ^{91}Rh decay

Moving further from stability, shell model predictions for levels in ^{91}Ru, shown in fig. 7 are less convincing.

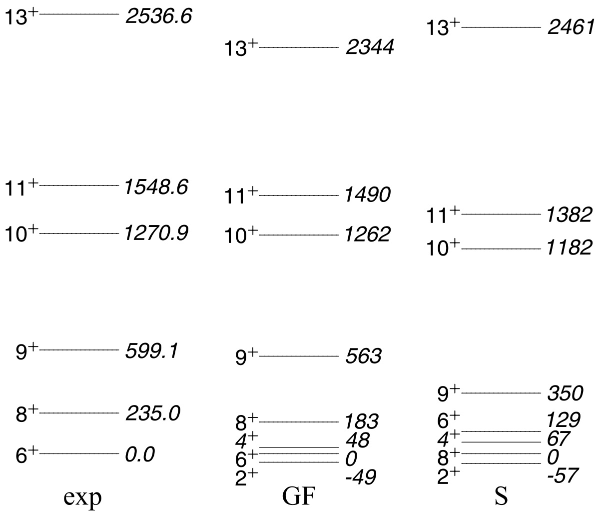

Fig. 12. The experimental high-spin level scheme of ^{92}Rh up to 13^+ [36] alongside shell model calculations of the yrast states up to the same spin.

Configurations of the $(\nu g_{9/2})^{-3}$ type provide the simplest low-lying single-particle excitations available to this nucleus. The $(13/2^+)$ level at 973 keV which is the only one observed prior to this [24,25], is well reproduced by both calculations. The 890 keV state, assumed to be the $11/2^+$ seen in ref. [26], is reasonably well reproduced by the GF calculation whereas the S calculation fails. The energy of the $1/2^-$ isomeric state is expected, on the basis of mass evaluations, to lie around 400 keV above the ground state [37]. The calculation using the parameters of Sinatkas predicts such a state at 386 keV and the GF calculation at 629 keV.

The larger discrepancy between experimental and calculated values in this case could be due to the fact that the effective interaction as determined by Sinatkas *et al.* from $N = 48$–50 nuclei in not correctly applicable to this $N = 47$ nucleus. In the more restricted model space, the effect of admixtures to the state wave functions from configurations outside the space should not be discounted. There is also the possibility that further from the $N = 50$ closed shell, collective excitations can become important and may influence low-lying excited states.

Regarding the 387 keV γ line, the first question to be asked is: to which nucleus does it belong? The fact that the line is not seen either without lasers (fig. 1(a)) or with the lasers tuned to the excitation scheme of ruthenium (fig. 1(c)), would tend to associate it with rhodium. Following this assumption, the shell model calculations of ^{91}Rh, shown in fig. 13 were performed to explore the possible origins of this decay. A study using the two-body matrix elements of Gross and Frenkel [38] of the $N = 46$ isotones with $Z = 40$–44 show good overall agreement between measured and calculated states. This together with the similarity between the two different calculations shown in fig. 13 may add weight to any conclusions. Both calculations show $1/2^-$ states at around 500 keV above a $9/2^+$ ground state. A number of possibilities thus present themselves; an $M4$ transition directly to the ground state or an $E3$ via the $7/2^+$ intermediate state calculated to lie at 126 and 157 keV. The slow rate of an $M4$ transition as predicted by the Weisskopf formula (> 70 min) and similar transitions in neighbouring nuclei rules out the first proposition. An $E3$ transition would be faster, the Weisskopf formula predicts 20 μs–2 ms however, similar transitions in the neighbouring nuclei show that these predictions can grossly underestimate measured values and a wide range of partial half-lives from ms to seconds is observed. The 387 keV line could thus be a candidate for the $(1/2^-) \rightarrow (7/2^+)$ transition with the subsequent $(7/2^+) \rightarrow (9/2^+)$ transition being too low in energy to be observed. An alternative scenario that the 387 keV line belongs to a similar de-excitation in ^{91}Ru involves the production of a ^{91}Rh $1/2^-$ isomeric state which then β decays followed by γ de-excitation to a $1/2^-$ state in ^{91}Ru.

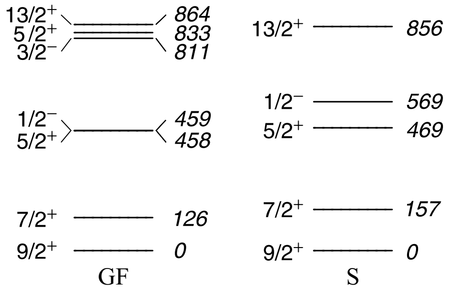

Fig. 13. Shell model calculations of excited negative- and positive-parity states in ^{91}Rh with $I^\pi \leq 15/5$ below 1 MeV.

Recent measurements [26,39] would appear to offer a way out of this predicament. A negative-parity band feeding a $(1/2^-)$ state in ^{91}Rh at an energy too low to accommodate a 387 keV transition was seen in ref. [39] effectively ruling out the first proposition that the 387 keV isomeric transition occurs in ^{91}Rh. Secondly, a low-lying $(7/2^+)$ state was seen in ^{91}Ru [26], indicating the GF calculations in fig. 7 to be the more reliable and enabling a $(1/2^-) \rightarrow (7/2^+) \rightarrow (9/2^+)$ cascade of which, because of its low energy, the $(7/2^+) \rightarrow (9/2^+)$ transition would go unseen in our detection setup. This leads to the conclusion that the $(1/2^-)$ isomer in ^{91}Rh is indeed populated in the heavy-ion fusion-evaporation reaction and subsequently β decays to negative-parity states in ^{91}Ru. The half-life of this $(1/2^-)$ state in ^{91}Ru has to be less than $\sim$ 200 ms [4,5] as the isomeric transition of 387 keV was not observed when the lasers were tuned to ruthenium (see fig. 1). The apparent half-life (1.46(11) s) must originate from the β decay of the $(1/2^-)$ isomer in ^{91}Rh. This half-life does not differ significantly from the $(9/2^+)$ value of 1.47(22) s, the three remaining γ lines from table 6 (438, 533 and 821 keV) cannot therefore be attributed uniquely to either the β decay of the $(9/2^+)$ or the $(1/2^-)$ isomer. From an extreme shell model picture, direct β decay to the $(1/2^-)$ isomer in ^{91}Ru is forbidden, involving as it does the transition $\pi(p_{1/2}^{-1}, g_{9/2}^{6})\nu g_{9/2}^{6} \rightarrow \pi g_{9/2}^{4}\ \nu(p_{1/2}^{-1}, g_{9/2}^{8})$. As a consequence, limits for the allowed $(9/2^+)$ ground state to $(9/2^+)$ ground state decay have been determined

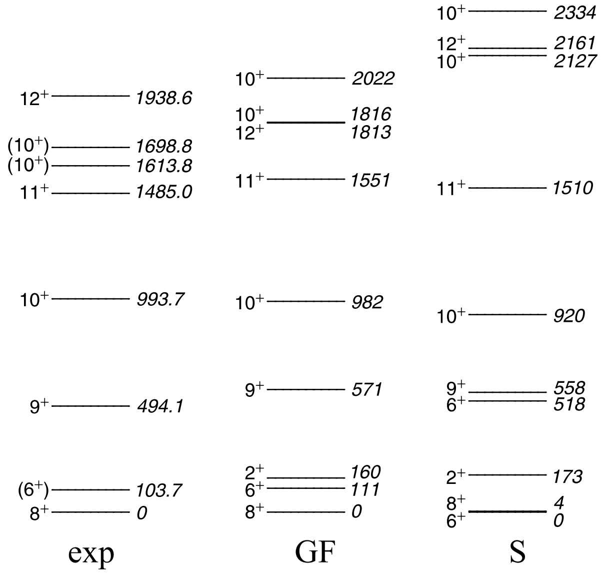

Fig. 14. The experimental high-spin level scheme of ^{90}Tc up to 12^+ [40] together with shell model calculations. Only yrast states from the calculations are included with the exception of the 10^+ where an addition state is added to correspond with the observed levels. The low-lying 2^+ states are included to show their position with respect to the ground state (cf. fig. 11).

depending on whether the three unplaced γ-rays are assumed to feed either the $(1/2^-)$ or the $(9/2^+)$ states in ^{91}Ru (see fig. 7). Note that these limits could change due to unobserved γ-rays (see sect. 4).

6.5 ^{91}Ru decay

The shell model calculations shown in fig. 9 show that the excited states in ^{91}Tc can be readily accounted for in terms of the shell model. Both calculations agree with the tentative I^π assignments.

6.6 ^{90}Ru decay

Regarding the odd-odd nucleus ^{90}Tc, the first property to be discussed is its ground-state spin. The $\pi g_{9/2}$ and $\nu g_{9/2}$ can couple to spins $I^\pi = 0^+$ to 9^+ of which it is argued, 8^+ is the ground state [40]. A study by Oxorn and Mark [41] identified two β-unstable states, a 1^+ and a (6^+) of which they claim the 1^+ to be the ground state. The shell model calculations in fig. 14 reproduce well the experimental data of Rudolph *et al.* [40] for excited states in ^{90}Tc below 2 MeV. All observed states are accounted for in the calculation with a difference, in most cases, of less than 100 keV. Both calculations favour a high-spin ground state and proffer a 2^+ at around 160 keV as a candidate for a low-spin isomer. However, the apparent strong feeding to this state conflicts with a 2^+ assignment. Clearly more experimental data is needed for this nucleus.

The good agreement between theory and experiment at high spin makes the situation at low spin all the more uncertain. The calculations shown next to the decay scheme in fig. 11 include levels with $I^\pi \leq 4^+$ with energies below 1 MeV. The lowest-lying 2^+ levels are those in fig. 14 at ~ 160 keV. The 1^+ levels calculated to lie around 700 keV may correspond to the observed 492.8 keV level however, the calculated lower levels are unable to provide a candidate for the 154.6 keV level which the observed feeding suggests has a spin and parity no greater than 2^+.

7 Conclusion and outlook

To summarise, elemental laser ionisation of reaction products, from heavy-ion fusion-evaporation, thermalised within a gas cell has been employed to produce the neutron-deficient ^{91,92,93}Rh and ^{90,91}Ru isotopes. The decay schemes have been determined from measurement of β-delayed γ decays and are discussed in terms of the shell model. Calculations were performed using the shell model code ANTOINE and with the interactions parameters of Gross and Frenkel as well as those in the larger model space of Sinatkas. With the exceptions of ^{90}Tc and to a lesser extent ^{91}Ru, the observed excited states are well reproduced by the calculations. Additional data on ^{90}Tc and ^{91}Ru would certainly elucidate the situation however, the considerable discrepancy between the GF and S calculations may be improved with the inclusion of new experimental information especially on the low-spin non-yrast states. The half-lives of the measured nuclei have been determined from fits to the time behaviour of their γ lines. Feature measurements include the lifetime and decay scheme of a low-spin β-decaying state in ^{92}Rh. By combining our data with recent in-beam measurements [26, 39], the β decay of a $(1/2^-)$ isomer populating eventually a 387 keV isomeric transition in ^{91}Ru has been observed.

As a complement to the measurements on β-delayed γ activity, a study of β-delayed proton activity was undertaken. These measurements were taken during a later experimental run in which technical difficulties led to rather low productions. However, upper limits for the branchings to proton-emitting states in their daughter nuclei were determined for the ^{90}Rh and ^{89}Ru precursors.

This work has demonstrated the successful application of on-line separation in combination with isotope production inside a gas cell to the neutron-deficient nuclei described here. The advent of high-efficiency detector technology [42] along with developments in radioactive ion beams anticipates continued work in this region and possible access to more exotic species in the direction of ^{100}Sn.

The authors are indebted to the technical support provided by J. Gentens and P. Van den Bergh. This work was made possible through support from the Inter-University Attraction Poles Research Program (IAP(P5/07)), the GOA Research Fund and FWO - Vlaanderen which are also acknowledged on behalf of K. Van de Vel. Members of the staff at GSI namely, H. Grawe, E. Roeckl and K. Burkard are thanked for their help and advice as well as the loan of the proton telescopes.

References

1. H. Herndl, B.A. Brown, Nucl. Phys. A **627**, 35 (1997).
2. P. Van den Bergh *et al.*, Nucl. Instrum. Methods B **126**, 194 (1997).
3. W. Reisdorf, Z. Phys. A **300**, 227 (1981).
4. Y. Kudryavtsev *et al.*, Nucl. Instrum. Methods B **114**, 350 (1996).
5. Y. Kudryavtsev *et al.*, Nucl. Instrum. Methods B **179**, 412 (2001).
6. P. Van Duppen *et al.*, Hyperfine Interact. **127**, 401 (2000).
7. L. Weissman *et al.*, Nucl. Instrum. Methods A **423**, 328 (1999).
8. `http://wwwinfo.cern.ch/asd/geant/`
9. `http://www.srim.org/`
10. `http://groups.nscl.msu.edu/lise/lise.html`
11. M. Facina *et al.*, to be published in Nucl. Instrum. Methods B.
12. `http://wwwinfo.cern.ch/asdoc/minuit/minmain.html`.
13. G. Audi, A.H. Wapstra, Phys. A **595**, 409 (1995).
14. A. Nilsson, M. Grececscu, Nucl. Phys. A **212**, 448 (1973).
15. S.E. Arnell *et al.*, Phys. Rev. C **49**, 51 (1994).
16. J.C. de Lange *et al.*, Z. Phys. A **279**, 79 (1976).
17. E. Nolte *et al.*, Z. Phys. A **298**, 191 (1980).
18. S.E. Arnell *et al.*, Z. Phys. A **346**, 111 (1993).
19. M. Górska *et al.*, Acta Phys. Pol. B **27**, 165 (1996).
20. C. Lingk *et al.*, Phys. Rev. C **56**, R2349 (1997).
21. S-H. Zhou *et al.*, Chin. Phys. Lett. **16**, 18 (1999).
22. P. Kienle *et al.*, Prog. Part. Nucl. Phys. **46**, 73 (2001).
23. P. Komninos *et al.*, Z. Phys. A **314**, 135 (1983).
24. S.E. Arnell *et al.*, Phys. Scr. **47**, 355 (1993).
25. J. Heese *et al.*, Phys. Rev. C **49**, 1896 (1994).
26. C. Rusu *et al.*, in preparation.
27. E. Hagberg *et al.*, Nucl. Phys. A **395**, 152 (1983).
28. D. Rudolph *et al.*, Phys. Rev. C **49**, 66 (1994).
29. Zhou Shuhua *et al.*, Z. Phys. A **350**, 7 (1994).
30. Li Zhankui *et al.*, Eur. Phys. J. A **5**, 351 (1999).
31. E. Caurier, F. Nowacki, Acta Phys. Pol. B **30**, 705 (1999).
32. R. Gross, A. Frenkel, Nucl. Phys. A **267**, 85 (1976).
33. J. Sinatkas *et al.*, J. Phys. G **18**, 1377 (1992).
34. J. Sinatkas *et al.*, J. Phys. G **18**, 1401 (1992).
35. F.J.D. Serduke *et al.*, Nucl. Phys. A **256**, 45 (1976).
36. D. Kast *et al.*, Z. Phys. A **356**, 363 (1997).
37. G. Audi *et al.*, Nucl. Phys. A **624**, 1 (1997).
38. E. Galindo *et al.*, Eur. Phys. J. A **9**, 439 (2000).
39. N. Marginean *et al.*, private communication.
40. D. Rudolph *et al.*, Phys. Rev. C **47**, 2574 (1993).
41. K. Oxorn, S.K. Mark, Z. Phys. A **303**, 63 (1981).
42. D. Habs *et al.*, Prog. Part. Nucl. Phys. **38**, 111 (1997).